Anomalous Orientation Behavior in a Series of Copoly(ester imide)s Observed by Wide-Angle X-ray Diffraction

Mark Leland, Zongquan Wu, Mukesh Chhajer, Rong-Ming Ho, and Stephen Z. D. Cheng*

Maurice Morton Institute and Department of Polymer Science, University of Akron, Akron, Ohio 44325-3909

Andrew Keller

H. H. Wills Physics Laboratory, The University of Bristol, Bristol BS8 1TL, U.K.

Hans R. Kricheldorf

Institut für Technische und Makromolekulare Chemie, Universität Hamburg, Bundesstrasse 45, D-20146 Hamburg 13, Germany

Received March 4, 1997; Revised Manuscript Received May 27, 1997[⊗]

ABSTRACT: A series of copoly(ester imide)s (CPEIs) was synthesized by the esterification of *N*,*N*′-dodecane-1,12-diylbis(trimellitimide) to two different acetylated diols, 4,4′-dihydroxybiphenyl and hydroquinone, in varying proportions. On the basis of their compositions, six samples are designated as CPEI(A−F), in which CPEI(A) is a homopolymer having 100% of incorporated 4,4′-dihydroxybiphenyl and CPEI(F), a homopolymer having 100% of incorporated hydroquinone. The composition ratios of the copolymers are 80/20 (B), 60/40 (C), 40/60 (D), and 20/80 (E). Except for CPEI(F), the five CPEI(A−E)s show enantiotropic liquid crystalline behavior during cooling from the isotropic melt. In all of the samples, highly ordered smectic crystal phases are assumed in the solid state. In the course of structural identification, it has been found that CPEI(A−E)s often exhibit anomalous wide-angle X-ray diffraction (WAXD) fiber patterns: the smectic layer normal is perpendicular to the fiber direction while the (*hk*0) reflections exhibit maxima along the meridian. Furthermore, the degree of orientation for the (*hk*0) reflections is apparently much lower than that of the layer structure. Crystallographic analysis is given to provide a quantitative explanation of experimentally obtained WAXD fiber patterns.

Introduction

It is known that poly(ester imide)s often exhibit thermotropic liquid crystalline behavior. This behavior may either be enantiotropic[1−3] or monotropic.[4−6] Recently, a series of copoly(ester imide)s (CPEIs) has been synthesized from the esterification of *N*,*N*′-dodecane-1,12-diylbis(trimellitimide) to two different acetylated diols, 4,4′-dihydroxybiphenyl and hydroquinone, in varying proportions. On the basis of variation of the composition, six samples are designated as CPEI(A−F), in which CPEI(A) is a homopolymer having 100% of the 4,4′-dihydroxybiphenyl-based ester group, and CPEI-(F) is a homopolymer having 100% of the hydroquinone based ester group. Following the alphabetic sequence, the composition ratios of the copolymers are 80/20 (B), 60/40 (C), 40/60 (D), and 20/80 (E) of the 4,4′-dihydroxybiphenyl and hydroquinone groups, respectively. The synthetic procedure and initial structural characterization of the homopolymers have been described previously.[7,8] These results demonstrated that CPEI(A) shows liquid crystalline behavior as well as anomalous fiber orientation involving an apparent perpendicular arrangement of the mesogen directors with respect to the fiber direction.[8] In fact, this anomalous phenomenon in molecular orientation has been reported by several authors for a few low molecular weight, thermotropic, main-chain liquid crystalline polymers.[9−12] Romo-Uribe and Windle recently found anomalous orientation in copolyesters synthesized from hydroxybenzoic acid (HBA) and hydroxynaphthoic acid (HNA) in dynamic shear experiments performed in the nematic state.[12] Their work concluded that the factors which affect this phenomenon include molecular weight, shear rate, and temperature.

In this publication, we discuss this anomalous molecular orientation phenomenon for a series of melt drawn CPEI fibers. In particular, detailed crystallographic analysis and calculation of the azimuthal intensity profile are described for comparison with experimental observations.

Table 1. Material Nomenclature and Inherent Viscosity

name	% biphenyl/% hydroquinone	η_{inh} (dL/g)[a]
A	100/0	N/A
B	80/20	0.94
C	60/40	0.48
D	40/60	0.58
E	20/80	0.40
F	0/100	0.34

[a] Inherent viscosity determined in 2 g/L solution in trifluoroacetic acid/methylene chloride (1:4).

Experimental Section

Materials and Samples. The series of CPEIs was prepared by the esterification of *N*,*N*′-dodecane-1,12-diylbis-(trimellitimide) to two different acetylated diols, hydroquinone and 4,4′-dihydroxybiphenyl, in varying proportions. The chemical structure of this series of CPEIs is shown below:

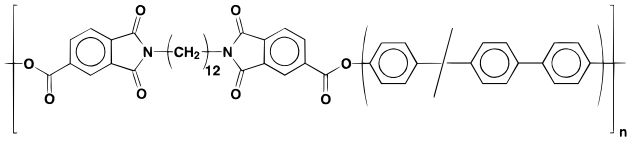

Table 1 shows the abbreviations for the system used in this publication as well as the proportions of the two ester groups

* To whom correspondence should be addressed.

[⊗] Abstract published in *Advance ACS Abstracts,* August 15, 1997.

S0024-9297(97)00299-4 CCC: $14.00 © 1997 American Chemical Society

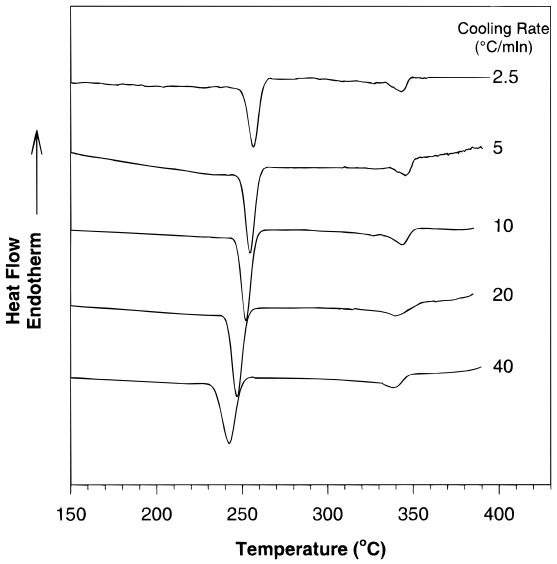

Figure 1. DSC cooling curves for CPEI(A) at different cooling rates.

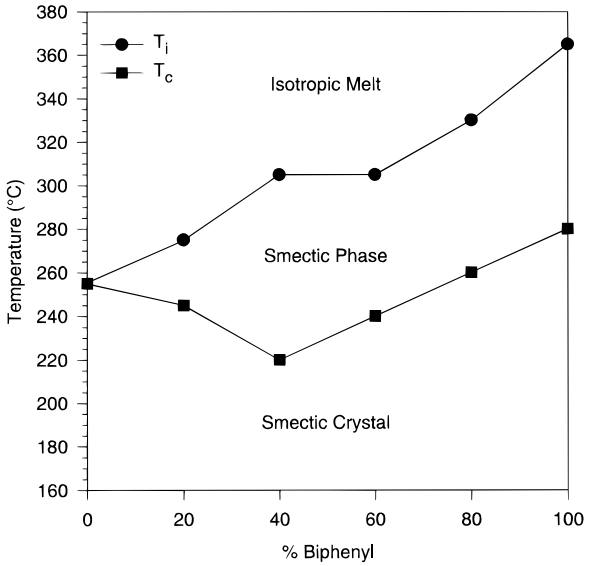

Figure 2. Phase boundary diagram based on composition of the biphenyl moiety.

and the inherent viscosities of the polymers taken from a 2 g/L solution of the polymer in dichloromethane/trifluoroacetic acid (4:1) at 20 °C. Note that for the material containing only the biphenyl moiety, CPEI(A), the inherent viscosity is not available due to the insolubility of this material.

Fibers of each CPEI sample were prepared by drawing from the liquid crystalline phase when applicable. Due to the limited tensile strength of the fibers, no further drawing was imposed on them although the fibers were annealed at elevated temperatures below the solid to liquid crystal transition temperatures.

Equipment and Experiments. Differential scanning calorimetry (DSC) was performed on a Perkin-Elmer DSC-7 with a cooling apparatus. The temperature and heat flow were calibrated using standard materials at different cooling rates between 2.5 and 40 °C/min.

Reflection wide-angle X-ray diffraction (WAXD) experiments were conducted with a Rigaku 12 kW rotating-anode generator (Cu Kα) and diffractometer. The X-ray beam was monochromatized using a graphite crystal. For WAXD powder patterns taken at room temperature, a scanning rate of 0.5°/min was used in the 2θ angle region ranging from 1.5 to 35°. The heating and cooling experiments were also conducted on this WAXD diffractometer equipped with a hot stage. The heating and cooling rates were 2 °C/min. The scanning rate in this case was 7.0°/min in the selected 2θ angle range. The reflection peak positions and widths observed from WAXD experiments were carefully calibrated using silicon crystals of known crystal sizes. Fiber WAXD patterns were obtained using a flat-plate vacuum camera attached to a Philips 2 kW tube X-ray generator. Fiber patterns were also collected using the rotating anode in conjunction with a Siemens area detector in order to perform azimuthal integrations.

Results and Discussion

Thermal Transitions and Structural Changes. Figure 1 shows a set of DSC cooling curves for CPEI(A) at different cooling rates (2.5−40 °C/min). Two exothermic transitions are apparent: a high temperature transition around 350 °C and a low temperature transition around 250 °C. Other CPEIs, except for CPEI(F), show very similar transition behavior during cooling. The high temperature transition peak does not exhibit significant cooling rate dependence. This is a clear indication that the transition may represent the formation of a low ordered liquid crystalline phase (nematic, smectic A, or smectic C phase) from the isotropic melt. Polarized light microscopy was used to confirm that the

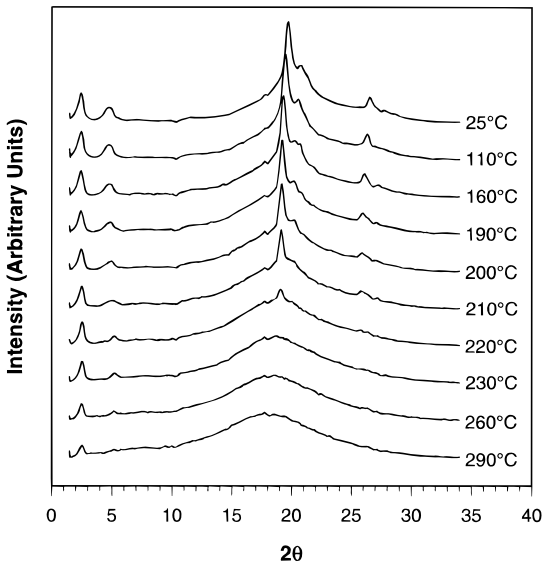

Figure 3. WAXD powder patterns of CPEI(C) during cooling at different temperatures.

samples have a transition from the isotropic state to a liquid crystalline phase at the higher exothermic peak temperatures observed in DSC. This liquid crystalline phase shows high birefringence and liquidlike viscosity under mechanical shearing. The second, low temperature exothermic peak shown in the DSC cooling experiments exhibits a slight cooling rate dependence. This transition may be associated with the formation of a highly ordered liquid crystal or crystal phase. For CPEI(F), only one exothermic process can be found during cooling, which corresponds to the low-temperature transitions observed in other CPEIs. The phase boundary diagram determined from DSC cooling data is shown in Figure 2.

Structural changes during cooling and heating can be observed from WAXD experiments. Figure 3 shows a set of cooling WAXD patterns for CPEI(C) as an example. Other CPEIs show similar results except for CPEI(F). It is evident that with decreasing temperature, structural changes occur which clearly correspond to the low-temperature thermal transitions found in DSC experiments. In the high temperature region

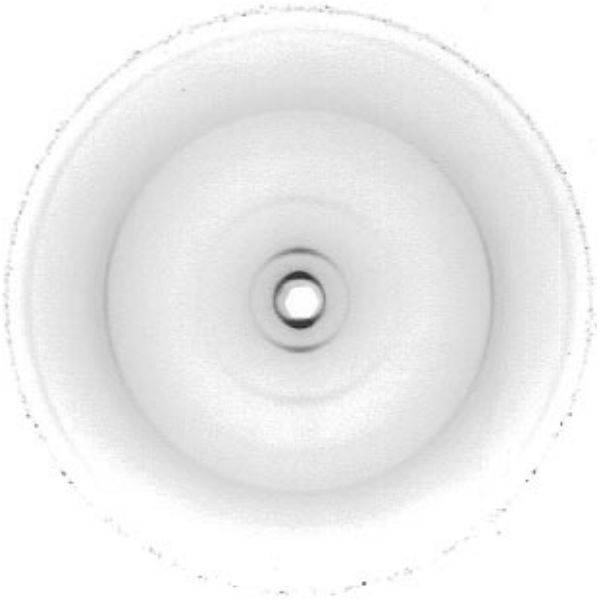

Figure 4. WAXD fiber pattern of CPEI(E) showing a normal fiber orientation. The fiber axis is vertical on the page.

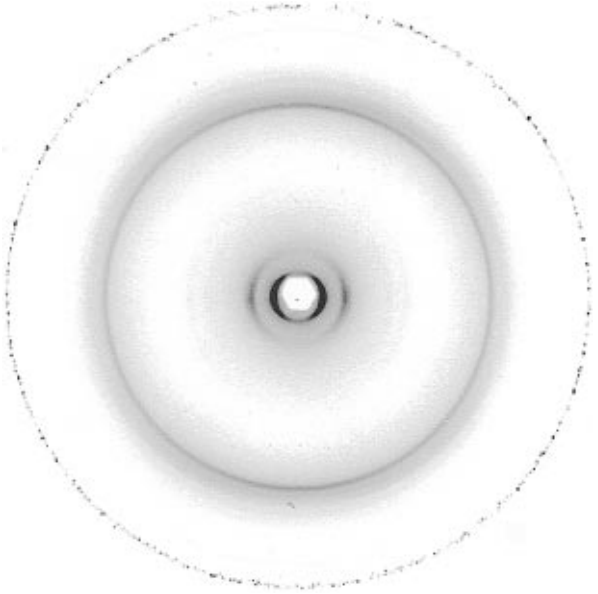

Figure 5. WAXD fiber pattern of CPEI(D) showing an anomalous fiber orientation. The fiber axis is vertical on the page.

below the isotropization temperature, two reflections are observed in the low-angle region below 6°. No reflection can be found in the high-angle region above 10°, indicating the absence of lateral packing order. If the low angle reflection is attributed to a layer structure periodicity, the WAXD powder pattern represents a typical low-ordered smectic A or C phase. After the temperature reaches the low transition temperature observed in DSC, the reflections can be seen not only in the low-angle region, but also in the high-angle region. This reveals that the low-temperature transition leads to the formation of lateral packing order between chain molecules. Of the reflections which appear at higher angles in Figure 3, the strong reflection at $2\theta = 19.9°$ most likely results from the (110) planes, while the weaker $2\theta = 21.1°$ reflection may be attributed to the (200) planes. The lateral packing appears to possess an orthorhombic lattice.[13] Detailed structure determination requires results obtained from WAXD fiber patterns and electron diffraction (ED) experiments combined with morphological observations which will be discussed elsewhere.[13]

Anomalous WAXD Fiber Patterns. CPEI(A−F) fibers generally exhibit a tendency to assume a fiber orientation in which the layer normal (the molecular chain axis) lies parallel to the fiber direction. Figure 4 provides an example for CPEI(E). Although the degree of orientation is relatively low due to the limited amount of sustainable draw for this series of materials, intensification of the lateral reflections [the (200) and (110) reflections] is apparent in the equatorial direction of the pattern. The layer reflection shows intensification on the meridian. This indicates that these CPEIs belong to the hexatic B, smectic crystal B, and smectic crystal E series of phases.[14,15]

However, under certain draw conditions, CPEI(A-E) fibers exhibit an orientation in which the layer reflection appears instead on the equator (Figure 5). This is similar to observations in sheared HBA/HNA copolyesters reported by Romo-Uribe and Windle.[12] In this case, the reflections representing the (*hk*0) planes (at high reflection angles) are apparently much more disoriented along the azimuthal angle (azimuthally diffuse) than the reflections representing the layers. However, integration along the azimuthal angle suggests that the (*hk*0) reflections are more intense on the meridian than the equator. This type of orientation as well as normal orientation (*i.e.*, lateral reflections appearing on the equator) can be found in materials CPEI(A-E) in which both types of orientation may sometimes appear in a single fiber. Materials containing a greater proportion of incorporated biphenyl seem to show an increased tendency to possess this anomalous orientation.

The anomalous pattern reveals a definite orientation of the layer normal in a direction perpendicular to the fiber axis. Furthermore, the meridional intensification of the (*hk*0) reflections suggests that the molecules are arranged perpendicular to the layers, which is consistent with fibers possessing normal orientation (Figure 4) as well as sheared samples examined with ED.[13] Therefore, the molecules appear to align perpendicular to the shear flow direction in the fiber forming process as described some years ago for relatively low molecular weight main-chain liquid crystalline polyesters.[9,10] However, the disoriented (azimuthally diffuse) nature of the (*hk*0) reflections obscures explicit evaluation of the molecular orientation.

Crystallographic Analysis of the Anomalous Fiber Patterns. As previously described, the orientation of the layer reflections in the anomalous pattern appears to be better than that of the (*hk*0) reflections within the same fiber (Figure 5). Although this appears to be inconsistent with conventional interpretation of fiber patterns, there is not necessarily a unique correlation between the orientation of different planes in a system of global cylindrical symmetry. The actual relation depends on the model adopted. In other words, the actual texture cannot be uniquely derived from pole figure mapping even in cases where mapping is complete (a situation which is seldom realized in a polymer system due to a limited number of often weak reflections in the diffraction patterns). Any such derivation explicitly or implicitly presupposes a model. In conventional fiber crystallography, the model implies a single axis of cylindrical symmetry (the fiber axis) with a prominent crystallographic direction (usually the chain direction or *c* axis) aligned along this direction. The

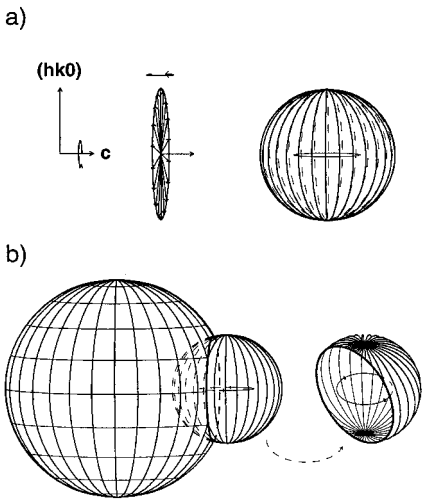

Figure 6. Model of symmetric layers oriented in the fiber forming process: (a) construction of the pole figure for the condition that the layer or lamellar normal (denoted as *c*) is confined to a direction perpendicular to the fiber direction; (b) intersection of the construct with the Ewald sphere of reflection and cut-away view of the intersected construct.

angles of inclination of other crystallographic directions (and the corresponding plane normals) are then defined by simple trigonometry through the geometry of the unit cell. If the orientation, in terms of the above model, is not perfect then there will be a certain spread with a specific distribution in the pole figure construction about the pole positions which correspond to perfect orientation. In such a situation, a simple relation should exist between the spreads of all of the poles (hence plane normals and reflections) which are involved. In other words, the orientation parameters (e.g. Hermann's orientation functions) will be related by the appropriate trigonometry.

However, other more complex models can exist which are still compatible with a global fiber symmetry but do not exhibit a simple relationship between the pole positions and their spread in orientation. In the case of Figure 5, we are clearly facing such a situation. Here, the precedent of flow induced texture in polyethylene (the "row structure") serves as a useful guide. In the row structure, the final pole figure results from two consecutive cylindrical randomizations around two mutually orthogonal "fiber" axes with the two operations not being commutative.[16,17] The resulting texture, seemingly complex as it may appear, is in fact a straight forward consequence of the underlying morphology and physical process giving rise to it. Specifically, in the row structure, the first direction is a prominent crystallographic direction corresponding to that of crystal growth. The second direction, the global fiber axis, is that of the overall orienting influence.

In the present case, just as in the row structure, the global fiber axis is that of the flow (i.e. shear) direction. The shear aligns the lamellar planes or smectic layers, causing the lamellar normals (i.e. *c* axis) to become oriented perpendicular to the flow. In the absence of a preferred direction within the orienting planes, all positions around the lamellar normal and, therefore, all positions of the (*hk*0) poles are possible. Thus, the first cylindrical randomization is performed around a fixed *c* direction leading to a pair of *c* poles and a circle of (*hk*0) poles at right angles to the *c* plane normals as shown on the left in Figure 6a. The second cylindrical averaging takes place around the flow/shear direction. This leads to an equatorial circle of *c* poles and a spread of (*hk*0) poles over the full pole figure with a specific distribution as shown on the right in Figure 6a. The (*hk*0) pole distribution is similar to the line density of longitudes on a globe, having maxima at the poles and minima along the equator. This pole distribution then translates into an X-ray diffraction pattern through the intersection of the whole construct with the Ewald sphere as shown in Figure 6b. The intersection for each spacing will then give the intensity distribution for the appropriate set of planes in the observed diffraction pattern. Thus, the (*hk*0) reflections will give continuous rings with maxima on the meridian and minima on the equator, while the (00*l*) reflections will be confined to the equator (i.e. a two-spot diffraction pattern).

The case discussed above represents the ideal case for perfect orientation in terms of the model adopted. Note that the spread in the (*hk*0) reflections is thus not a sign of disorientation as would be suggested by conventional interpretation, but is intrinsic to the model in its maximum perfection. Any genuine disorientation, in terms of the model, would then superpose its own broadening on this intrinsic spread. A measure of such a disorientation (i.e. departure from the perfect orientation in terms of the model) is provided by the arc spread of the (00*l*) reflections, which then translates in a calculable way (next section) to the corresponding spreads in the (*hk*0) reflections.

At this stage we conclude that the qualitative features of the anomalous diffraction patterns can be accounted for by the model arising from the alignment of the smectic layer or lamellar planes along the flow direction. This implies a perpendicular alignment of the chains, with no preferred direction for the (*hk*0) reflections within the planes. The factors which govern the process and lead to the anomalous orientation of these samples are presently not fully understood but merit further investigation. Other researchers have cited molecular weight, temperature, and shear rate as factors which have an effect on this phenomenon.[12] We expect that these factors may also play an important role in our system. Below we proceed with a more quantitative test of this model.

Quantitative Calculation and Simulation. In order to provide a quantitative description of the analysis proposed above, a mathematical formulation has been conducted to describe the azimuthal profile of the lateral (*hk*0) reflections. Two methods (analytical and computational) were used to determine the azimuthal intensity profile based on the model. The analytical method employs a continuous function to describe the intensity at any specified angle. The computational (numerical) method relies on the generation of points on the surface of the pole distribution at discrete intervals, followed by evaluation and summation of intersecting points in order to obtain the density of points which intersect the Ewald sphere of reflection. Code for the computational model was written and executed using the Perl programming language.

In order to evaluate the azimuthal intensity profile, it is first necessary to calculate the intersection between the (*hk*0) pole distribution and the sphere of reflection. For a spherical construct ($r = 1/d$) centered at the origin of an arbitrary Cartesian coordinate system and a sphere of reflection ($r = 1/\lambda$) centered at $(0,1/\lambda,0)$ of the same coordinate system, the equation of the circle of intersection is given as

$$x^2 + z^2 = \frac{1}{d^2} - \frac{\lambda^2}{4d^4} \tag{1}$$

$$y = \frac{\lambda}{2d^2} \tag{2}$$

where λ is the wavelength of incident radiation and d is the d-spacing of the relevant ($hk0$) planes.

Analytically, if the longitudinal lines of the construct are evaluated as a flux (q), the flux density can be evaluated at any point along a line. Assuming that the flux density at a point intersecting the sphere of reflection is directly proportional to the intensity of the reflection at that point, the following equation may be used to calculate the intensity at any point along a given latitudinal line:

$$I(\gamma) = \frac{Kq}{2\pi\frac{1}{d}\cos\gamma} \tag{3}$$

where K is the constant of proportionality, $1/d$ is the radius of the construct, and γ is the angle between the vector describing the point and the equatorial plane. The intensity may be expressed in terms of the azimuthal angle (ϕ) by establishing the geometric relationship between γ and ϕ:

$$I(\phi) = \frac{Kq}{2\pi\frac{1}{d}\cos\left[\arcsin\left(\frac{1}{2}\sin(\phi)\sqrt{4 - \frac{\lambda^2}{d^2}}\right)\right]} \tag{4}$$

A plot of an azimuthal profile is shown in Figure 7. For this plot $q = 5762$, $K = 1$, $\lambda = 0.1542$ nm, and $d = 0.45$ nm.

The same result may be obtained by a computational reproduction of the symmetry operations used to arrive at the construct. The ($hk0$) pole distribution is calculated by assigning an arbitrary initial vector representing a lateral ($hk0$) reflection and creating a set of points by rotation around the two axes of symmetry described above at a regular interval. Namely, a set of points is generated by rotating the vector 360° around the fiber axis at a specified step angle ($d\theta$) generating a latitude line on the construct. The vector is then rotated one step ($d\theta$) around the axis describing the normal to the layer and again rotated 360° around the fiber axis. The process is repeated until the entire ($hk0$) pole distribution is generated as a series of latitude lines. Due to the nature of the intersection, if the coordinate system is chosen as described above, all points lying on the circle described by eq 1 have the same y coordinate as specified by eq 2. Hence, points which fell within a narrow range of y (dy) at the specified y were recorded with respect to their azimuthal positions at 1° intervals along ϕ. In order to impose a Gaussian distribution on the system, it is necessary to define another parameter (ψ) which represents the angle between the normal to the layer and the plane perpendicular to the fiber axis (xy-plane). Figure 7 also shows the computational result of a calculation made with $\psi = 0$, $y = 0.381$ nm^{-1}, $dy = \pm 0.004$ nm^{-1}, $d = 0.45$ nm, $\lambda = 0.1542$ nm, and a step size ($d\theta$) of 0.01°.

Figure 7 provides a comparison of the azimuthal profiles generated by these two methods. The value of q was arbitrarily chosen in order to shift the results into coincidence for easier comparison. Clearly, both methods arrive at virtually the same profile. There are several important features to note. At an azimuthal angle of 90° (representing the meridian of the fiber pattern) there is a strong, relatively sharp peak in the intensity. On the other hand, the pattern approaches a minimum value at the equator. The intensity does not reach zero anywhere along the azimuthal angle. Hence, evaluation of the Hermann's orientation function for the ($hk0$) reflection yields a value of $f_\phi = 0.18$ even for perfect orientation of the axis describing the layer normal.

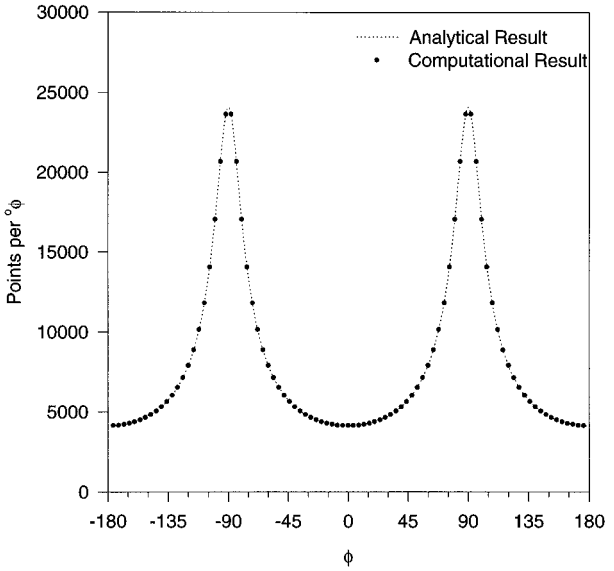

Figure 7. Plot of the azimuthal intensity profile for the ($hk0$) reflection where $\psi = 0$ calculated using the analytical and computational models.

In order to account for imperfect orientation in our model, we shall consider the effect of a spread in orientation of the c axis with respect to an ideal perpendicular orientation to the global fiber axis. It should be noted that the spread of the c poles need not translate uniquely into a corresponding spread in the ($hk0$) poles even when computed *via* the two-step cylindrical averaging of the model. Namely, there are an infinite range of choices between two extremes. In the first extreme, the second axis of cylindrical averaging may be chosen such that it is always normal to the global fiber axis in which case it will no longer be equivalent to c for all crystals. In the opposite extreme, second, the c axis may be retained as the second axis of cylindrical averaging in which case this axis will also have an orientation distribution. All intermediates between these two extremes exist as possible alternatives illustrating the indefiniteness intrinsic to such texture problems. For the sake of simplicity we shall adopt the second case in what follows.

In order to quantitatively evaluate imperfect orientation in this manner, a Gaussian distribution function was imposed on the results from multiple calculations made on systems with various tilt angles (ψ). The ψ values ranged from 0 to 89.5° and a step of 0.5° was used. To reduce computation time, a step size ($d\theta$) of 0.15° was utilized in generating the pole figure construct. The increased step size results in a certain degree of scatter in the calculated data, and the data are smoothed for easier comparison. Other than the step size and variation in ψ, all parameters are the same as described for Figure 7.

The results of the computation are shown in Figure 8 for three different standard deviations (σ). It appears

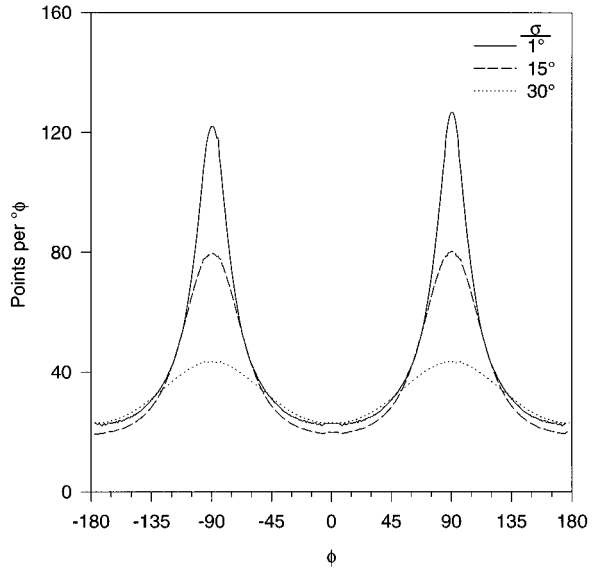

Figure 8. Plot of the azimuthal intensity profiles for the (*hk*0) reflections for systems with three different standard deviations ($\sigma = 1$, 15, and 30°, respectively) imposed on the ψ parameter.

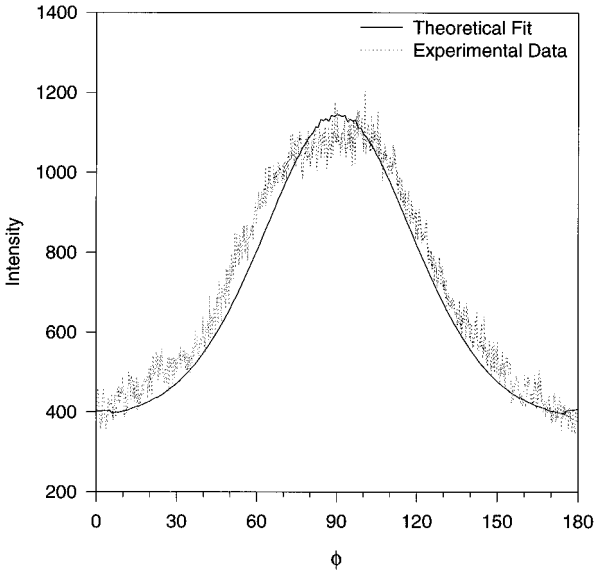

Figure 9. Plot of the azimuthal intensity profile determined theoretically and experimentally for CPEI(D).

that as the standard deviation increases there is an increase in the breadth of the azimuthal intensity centered at the meridian. On the other hand there seems to be little effect on the intensity at the equator. Calculations based on the computational model can be compared to the experimental results. Integration was performed along the azimuthal angle for the second order layer reflection of a fiber pattern from CPEI(D) (Figure 5). The integrated intensity was then fit with a Gaussian distribution as an approximation. The Gaussian fit exhibited a standard deviation (σ) of approximately 21°. This standard deviation was then used to calculate the azimuthal intensity profile of the (*hk*0) reflections by imposing the distribution for the layer reflections on the ψ parameter. The azimuthal profile of the (110) and (200) reflections was determined by integration along the azimuthal angle within the appropriate 2θ range for the same fiber pattern. The experimental and calculated profiles can then be compared after appropriate scaling of the calculated profile ($q = 19.5$ was used to shift the curves into coincidence). Figure 9 shows a comparison of the two profiles from $\phi = 0°$ to $\phi = 180°$ (the second half of the experimental profile was skewed by the presence of the beam stop). The proximity of these two curves suggests a reasonable correspondence between the experimental and calculated profiles.

Conclusion

Materials CPEI(A−E) show enantiotropic smectic liquid crystalline phases which appear to be associated with the formation of anomalous orientation in the fiber drawing process. This anomalous orientation is characterized by an orientation of the layer normal in a direction perpendicular to the fiber direction. The tendency to assume this orientation increases as the percent of incorporated biphenyl increases in the copolymers. A model has been constructed for the pole figure of the system based on the orientation of lamella or smectic layers. The model is consistent with fiber patterns in that the degree of orientation of the layer reflection appears to be better than that of the (*hk*0) reflections. Quantitative evaluation of the model shows that for perfect orientation of the layer reflection, the expected degree of orientation for the lateral reflection is comparatively low. By calculating the distribution function from integration around the azimuthal angle of the layer reflection, a computational model of the system can be used to predict with relative accuracy the orientation in the (*hk*0) reflections.

Acknowledgment. This work was supported by the Division of Materials Research, National Science Foundation (DMR-9617030). We also wish to thank the late Professor, Dr. H. G. Zachmann for his insight and discussion on the topic.

References and Notes

(1) Kricheldorf, H. R.; Jahnke, P. *Eur. Polym. J.* **1990**, *26*, 1009.
(2) Kricheldorf, H. R.; Pakull, R.; Buchner, S. *J. Polym. Sci., Polym. Chem.* **1989**, *27*, 431.
(3) de Abajo, J.; de la Campa, J.; Kricheldorf, H. R.; Schwarz, G. *Makromol. Chem.* **1990**, *191*, 537.
(4) Pardey, R.; Zhang, A.; Gabori, P. A.; Harris, F. W.; Cheng, S. Z. D.; Adduci, J.; Facinelli, J. V.; Lenz, R. W. *Macromolecules* **1992**, *25*, 5060.
(5) Pardey, R.; Shen, D.; Gabori, P. A.; Harris, F. W.; Cheng, S. Z. D.; Adduci, J.; Facinelli, J. V.; Lenz, R. W. *Macromolecules* **1993**, *26*, 3687.
(6) Pardey, R.; Wu, S. S.; Chen, J.; Harris, F. W.; Cheng, S. Z. D.; Keller, A.; Adduci, J.; Facinelli, J. V.; Lenz, R. W. *Macromolecules* **1994**, *27*, 5794.
(7) Kricheldorf, H. R.; Pakull. R. *Polymer* **1987**, *28*, 1772.
(8) Kricheldorf, H. R.; Pakull, R. *Macromolecules* **1988**, *21*, 551.
(9) Krigbaum, W. R.; Ciferri, A.; Acierno, D. *J. Appl. Polym. Phys. Appl. Polym. Symp.* **1985**, *41*, 293.
(10) Krigbaum, W. R.; Watanabe, J. *Polymer* **1983**, *24*, 1299.
(11) Alt, D. J.; Hudson, S. D.; Garay, R. O.; Fujishiro, K. *Macromolecules* **1995**, *28*, 1575.
(12) Romo-Uribe, A.; Windle, A. H. *Macromolecules* **1996**, *29*, 6246.
(13) Leland, M.; Cheng, S. Z. D.; Kricheldorf, H. R. Manuscript in preparation.
(14) Gray, G. W.; Goodby, J. W. G. *Smectic Liquid Crystals*; Leonard Hill: London, 1984.
(15) Pershan, P. S. *Structure of Liquid Crystal Phases*; World Scientific: Singapore, 1988.
(16) Keller, A. *J. Polymer Sci.* **1955**, *15*, 31.
(17) Keller, A.; Machin, M. J. *J. Macromol. Sci. (Phys.)* **1967**, *B1*, 41.

MA970299E